EPJ Web of Conferences **17**, 04002 (2011)
DOI: 10.1051/epjconf/20111704002

Quasifission and Fusion-Fission Competition in ^{32}S + ^{184}W Reaction

H. Q. Zhang[1,a], C. L. Zhang[1], C. J. Lin[1], Z. H. Liu[1], F. Yang[1], A. K. Nasirov[2], G. Mandaglio[3], M. Manganaro[3], and G. Giardina[3]

[1] China Institute of Atomic Energy, P. O. Box 275(10) 102413 Beijing
[2] Joint Institute for Nuclear Research, 141980 Dubna, Russia
[3] Dipartimento di Fisica dell' Università di Messina, 98166 Messina, and Istituto Nazionale di Fisica Nucleare, Sezione di Catania, Italy

Abstract. The angular distribution of fission fragments for the ^{32}S+^{184}W reaction at center-of-mass energies of 118.8, 123.1, 127.3, 131.5, 135.8, 141.1 and 144.4 MeV were measured. The experimental fission excitation function is obtained. The fragment angular anisotropy is found by extrapolating the fission angular distributions. The measured fission cross sections are decomposed into fusion-fission, quasifission and fast-fission contributions by the dinuclear system model. The total evaporation residue and fusion-fission excitation functions are calculated in the framework of the advanced statistical model.

1 Introduction

Studies of fusion-fission reactions between heavy ion projectile and heavy target nuclei have demonstrated to be very useful in developing an understanding of the nuclear reaction dynamics. Especially with the development of radioactive nuclear beams and the superheavy element synthesis, this study is becoming a hot topic again [1–4]. In this paper we have analyzed the angular distributions of fission fragments of the ^{32}S+^{184}W reaction and we obtained fission excitation functions. The fragment angular anisotropies $A_{\rm exp}$ are found by extrapolating the fission angular distributions to angles 0° and 90° by the method used in Ref. [5]. Then, the mean square angular momentum $\langle L^2\rangle$ values were obtained. Hereafter we use for simplicity ℓ from the definition $L = \ell\hbar$. We assumed the calculated capture cross sections to be equal to the experimentally measured cross section for fission-like fragments, and further decompose the measured fission cross section into fusion-fission, quasifission and fast fission contributions by the dinuclear system model [6].

2 Experimental procedure

The experiment was performed at HI-13 tandem accelerator of China Institute of Atomic Energy, Beijing. A collimated ^{32}S beam with incident energies $E_{\rm lab}$=140, 145, 150, 155, 160, 165 and 170 MeV bombarded a target of ^{184}W which was mounted at center of the scattering chamber. Data from Si strip detectors were recorded in the coincidence mode and are shown in Fig. 1. In fitting the angular distributions of the fission fragments we used the familiar expression as in Ref. [5]:

$$W(\theta) = \sum_{J=0}^{J_{\max}} \frac{(2J+1)^2 \exp[-(J+\frac{1}{2})^2 \sin^2\theta/4K_0^2] J_0[i(J+\frac{1}{2})^2 \sin^2\theta/4K_0^2]}{\mathrm{erf}[(J+\frac{1}{2})/(2K_0^2)^{1/2}]} \quad (1)$$

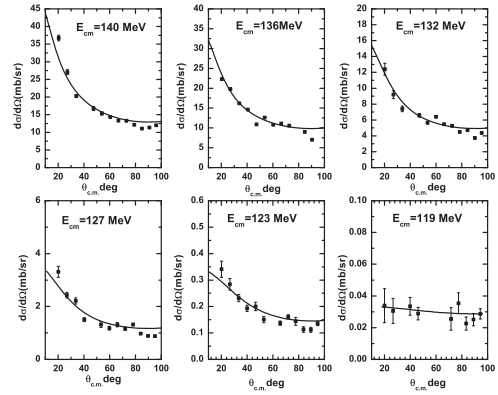

Fig. 1. Fissionfragment angular distributions for the ^{32}S+^{184}W reaction at different energies as indicated.

assuming M=0, *i.e.* assuming the spins of the target and projectile were zero. J_0 is the zero order Bessel function with imaginary argument and error function erf(x) is defined as

$$\mathrm{erf}(x) = (2/\pi^{1/2}) \int_0^x \exp(-t^2)dt. \quad (2)$$

$J_{\max}$ is obtained by reproducing the capture cross section. The K_0^2 value is found by fitting the angular distribution at known $J_{\max}$ from the total fission cross section. It is seen from Fig. 1 that the anisotropy of angular distribution increases with increasing collision energy $E_{\rm c.m.}$.

The measured values of $\sigma_{\rm capture}$ and the deduced experimental values of $A_{\rm exp}$, K_0^2 and $\langle L^2\rangle$ for the ^{32}S+^{184}W reaction are presented in Table 1. The capture cross sections are shown in Fig. 2 where they are compared with the theoretical results. The total fission cross section is assumed to be equal to the theoretical capture cross section and it was de-

[a] e-mail: Huan@ciae.ac.cn

Table 1. The measured capture cross sections and the deduced experimental values of $A_{\rm exp}$, K_0^2 and $\langle L^2\rangle$ for the ^{32}S+^{184}W reaction. The $E_{\rm c.m.}$ are the center of mass energies calculated at the center of the target.

$E_{\rm c.m.}$ (MeV)	$E^*_{\rm CN}$ (MeV)	$\sigma_{\rm capture}$ (mb)	$A_{\rm exp}$	K_0^2 ($\hbar^2$)	$\langle L^2\rangle$ ($\hbar^2$)
118.8	37.2	0.04	1.51	114.71	234
123.1	41.5	2.35	2.16	124.35	577
127.3	45.8	22.97	2.27	132.09	671
131.5	50.0	81.01	2.74	140.01	975
135.8	54.3	132.27	3.06	148.67	1225
141.1	58.5	189.33	3.28	157.35	1435
144.4	61.8	237.06	3.8	155.09	1737

composed into fusion-fission and quasifission in the framework of the dinuclear system model (DNS) mentioned.

3 Theoretical description and comparison with measured data

The calculations were performed for the $E_{\rm c.m.}$=119.5–149.5 MeV energy range and initial values of the orbital angular momentum ℓ =0–120. Due to the deformed shape of ^{184}W (β_2 = 0.24 and β_4 = −0.095) in the ground state we included in our calculations a dependence of the excitation function of capture, complete fusion and quasifission on the orientation angle α_T of its axial symmetry axis. The ground state shape of ^{32}S is spherical but the quadrupole (2^+) and octupole (3^-) collective excitations in spherical nuclei are taken into account as amplitudes of the zero-point motion mode of surface vibration. The deformation parameters of the first excited quadrupole state $\beta_2^{(2+)}$ = 0.312 (taken from Ref. [8]) and the ones of the first excited octupole state $\beta_3^{(3-)}$=0.41 (taken from Ref. [9]). The final results of the capture and complete fusion are obtained by averaging the contributions calculated for the different orientation angles (α_T=0, 15, 30, ..., 90°) of the symmetry axis of the target nucleus:

$$\langle\sigma_{\rm fus}(E_{\rm c.m.},l)\rangle = \int_0^{\pi/2} \sin\alpha_T \sigma_{\rm fus}(E_{\rm c.m.},l;\alpha_T)d\alpha_T. \quad (3)$$

This methods were developed and used in the Refs. [10]. The results of calculation of the excitation functions are presented in Fig. 2. The agreement between the experimental and theoretical capture cross sections was reached by adjusting the radius parameter C_R entered to rescale the nuclear radius:

$$R_1 = C_R\sqrt{(R_{\rm p}^2 Z_1 + R_{\rm n}^2(A_1 - Z_1))/A_1}\,, \quad (4)$$

where $R_{\rm p}$ and $R_{\rm n}$ are the proton and neutron radii, respectively, obtained from Ref. [11]:

$$R_{\rm p} = 1.237(1 - 0.157(A-2Z)/A - 0.646/A)A^{1/3}, \quad (5)$$

$$R_{\rm n} = 1.176(1 + 0.25(A-2Z)/A + 2.806/A)A^{1/3}. \quad (6)$$

The presented results are obtained at C_R = 0.925 for all values of $E_{\rm c.m.}$. Using Eq.(3) we calculated the partial fusion cross sections which were used to estimate the cross sections of ER and fusion-fission by the advanced statistical model[12–14]. Taking into account the dependence of the fission barrier ($B_{\rm f}$) of the rotating compound nucleus (CN) on its angular momentum we found a value of ℓ at which $B_{\rm f}$ disappears using the rotating finite range model by A. J. Sierk: $\ell_{\rm B}$=68. Then we calculate the fast fission contribution for $\ell > \ell_{\rm B}$

$$\sigma_{\rm fast\,fission}(E_{\rm c.m.}) = \sum_{\ell=\ell_{\rm B}}^{\ell=\ell_{\rm max}} (2\ell+1)\sigma_{\rm fus}(E_{\rm c.m.},\ell) \quad (7)$$

where $\ell_{\rm max}$ is the maximum value of angular momentum of the dinuclear system for the given value of $E_{\rm c.m.}$. The value of $\ell_{\rm max}$ is found by solving the equations of motion for the radial distance and orbital angular momentum with the given values of $E_{\rm c.m.}$, ℓ_0 and $R_{\rm max}$ = 20 fm.

In Fig. 2 are also presented the total fusion-fission and ER cross sections obtained by the advanced statistical model, and references therein) describing the full deexcitation cascade of the ^{216}Th* CN formed in the ^{32}S+^{184}W reaction. The code takes into account the competition between evaporation of light particles (n, p, α, and γ) and fission processes along each step of the deexcitation cascade of CN. The effective fission barrier for CN and intermediate excited nuclei along the cascade are obtained taking into account the macroscopic fission barrier, predicted by the rotating droplet model as parameterized by Sierk, together with the microscopic corrections allowing for the angular momentum and temperature fade-out of shell corrections to the fission barrier.

The cross section of ER formed at each step x of the deexcitation cascade after the emission of $\nu(x)$n+$y(x)$p+$k(x)\alpha$+ $s(x)\gamma$ particles (ν, y, k, s are numbers of neutrons, protons, α-particles and γ-quanta) from the hot CN is calculated by the formula[6]:

$$\sigma_{\rm ER}(E_x^*) = \sum_{Z_l=0}^{l_d} \sigma^l_{(x-1)}(E_x^*) W_{{\rm sur}(x-1)}(E_x^*, l), \quad (8)$$

where $\sigma^l_{(x-1)}(E_x^*)$ is the partial cross section of the intermediate nucleus formation at the $(x-1)^{th}$ step and $W_{{\rm sur}(x-1)}(E_x^*,\ell)$ is the survival probability of the $(x-1)$th intermediate nucleus against fission along the deexcitation cascade of CN; E_x^* is an excitation energy of the nucleus formed at the xth step of the deexcitation cascade. It is clear that $\sigma^l_{(0)}(E_0^*) = \sigma^l_{fus}(E^*)$ at $E^*_{CN} = E^*_0 = E_{\rm c.m.} + Q_{\rm gg}$, where $Q_{\rm gg}$ is energy balance of reaction. The numbers of the being emitted neutrons, protons, α-particles, γ-quanta, $\nu(x)$n, $y(x)$p, $k(x)\alpha$, and $s(x)\gamma$, respectively, are functions of the step x. The emission branching ratio of these particles depends on the excitation energy and angular momentum of the being cooled intermediate nucleus $A = A_{\rm CN} - (\nu(x) + y(x) + 4k(x))$ and $Z = Z_{\rm CN} - (y(x) + 2k(x))$ [6]. We note that in Fig. 2 the maximum value of the cross section of the evaporation residues is about 0.12 mb and the complete spectrum is contributed mainly by the evaporation of charged particles which are accompanied with a small number of neutrons along the deexcitation cascade of CN.

We present the calculated values of $P_{\rm CN}$ as a function of the beam energy in Fig. 3. It is seen that the hindrance to fusion is strong at very small and large values of the collision energy $E_{\rm c.m.}$. The yield of quasifission is dominant at the sub-barrier beam energies leading to capture of

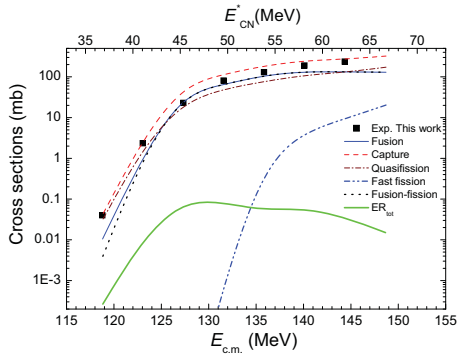

Fig. 2. Comparison of the experimental data with theoretical results.

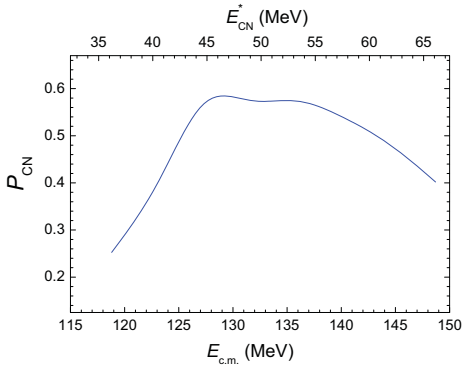

Fig. 3. Theoretical value of $P_{CN}(Z)$ for $^{32}S+^{184}W$ system.

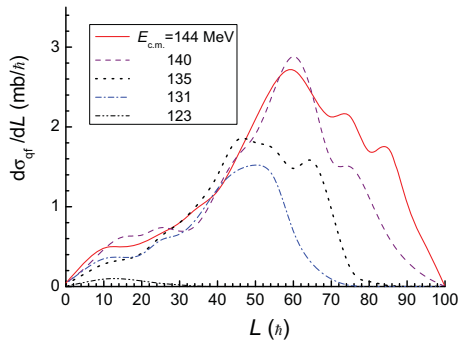

Fig. 4. The partial quasifission angular momentum distributions calculated at different incident energies $E_{c.m.}$ for the $^{32}S+^{184}W$ reaction.

deformed nuclei only with the small orientation angle of its symmetry axis relative to the beam direction.The decrease of its values at collision energies $E_{c.m.} > 135$ MeV is explained by decrease of the quasifission barrier B_{qf} as a function of the orbital angular momentum ℓ. At the same time the intrinsic fusion barrier B^*_{fus} increases with increasing ℓ.

It is seen from Fig. 4 that the values $\ell > 45$ are populated at collision energies $E_{c.m.} > 135$ MeV. Therefore, we conclude that the contribution of quasifission becomes dominant at $E_{c.m.} > 135$ MeV and it has an effect on the anisotropy of angular distribution which increases with increasing the collision energy. The decrease of P_{CN} at larger energies is explained by the decrease of the quasifission barrier B_{qf} by increasing ℓ in collisions with all orientation angles. To clarify the role of quasifission fragments

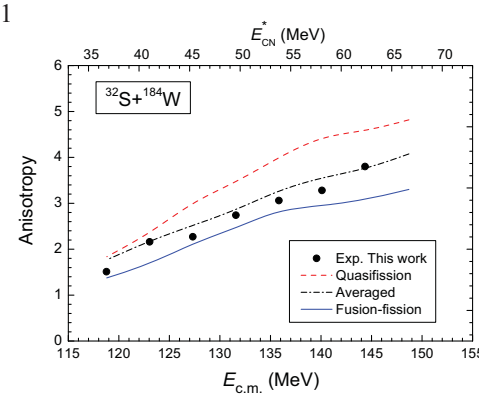

Fig. 5. Comparison of the anisotropies measured with the theoretical results.

in the observed anisotropy A_{exp}, we calculated the contributions of the quasifission (A_{qf}) and fusion-fission (A_{CN}) fragments.

In Fig. 5 we compare the anisotropy measured (circles) in this work with the theoretical results for the anisotropy of the quasifission (dashed line) and fusion-fission (solid line) fragments as a function of the center-of-mass energy (bottom axis) and excitation energy of the CN (top axis). The averaged theoretical anisotropy over the contributions of both mechanisms are presented by the dot-dashed line. It is seen that the averaged values of anisotropy are closer to the experimental data A_{exp}. Consequently we confirm that the measured cross section of the fission fragment formation and their angular distribution are results of mixing of the quasifission and fusion-fission products. In the upper panel of Fig.6, we compare experimental and theoretical values of mean square values of angular momentum. The experimental $\langle L^2\rangle$ values are obtained from the measured anisotropy A_{exp} and K_0^2 values used to fit measured angular distributions presented in Fig. 1. The theoretical values for fusion-fission and quasifission fragments are calculated by averaging ℓ^2 using the partial cross sections of the quasifission (dashed line) and complete fusion (solid line) events. The experimental data are well described with the averaged values of L^2 between the complete fusion and quasifission cross sections:

$$\langle L^2\rangle = \frac{(\sigma_{fus}\langle L^2\rangle_{fus} + \sigma_{qf}\langle L^2\rangle_{qf})}{\sigma_{fus} + \sigma_{qf}}. \qquad (9)$$

In the lower panel of Fig.6, the experimental results of K_0^2 are compared with the theoretical values obtained from the description of A_{exp} (dashed line in Fig.5) and $\langle L^2\rangle$ (dot-dashed line in Fig.6) extracted from the experimental angular distributions. The comparison shows again the dominance of the quasifission fragments into measured data at low energies.

4 Conclusion

In summary, the fission-fragment angular distributions for the $^{32}S+^{184}W$ reaction have been measured over a wide energy range. We obtained the cross sections for fission-like products, the fission-fragment anisotropy and extracted the mean square angular momentum $\langle l^2\rangle$. These values are compared with the results of the DNS model calculations. Assuming the measured fission cross sections is equal to the capture cross section they were decomposed into fusion-fission, quasifission and fast fission contributions using the

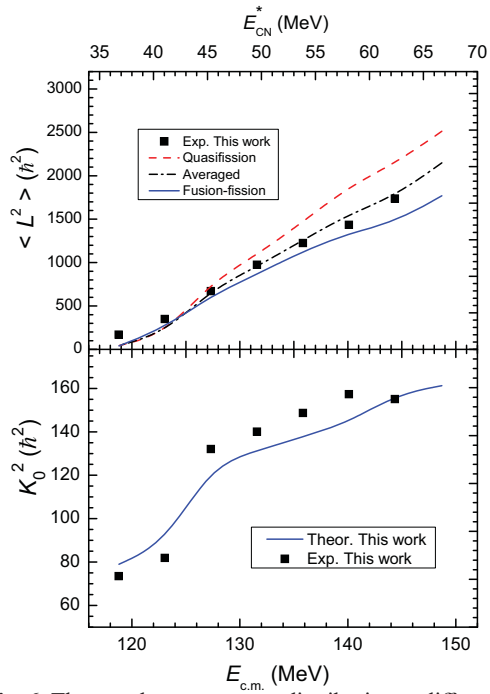

Fig. 6. The angular momentum distribution at different center-of-mass energies and theoretical predictions (see the text).

dinuclear system model. The hindrance to complete fusion at small collision energies increases due to the increase of the quasifission events and it is explained by the elongated shape of the dinuclear system which is formed in collisions with small orientation angle of the symmetry axis of ^{184}W with respect to the beam direction. Because of collisions with small orientation angles the intrinsic fusion barrier B^*_{fus} is larger and quasifission barrier B_{qf} is smaller in comparison with the corresponding barriers in the case of collisions with large orientation angles. An increase of the quasifission contribution at large beam energies is connected with the angular momentum dependence of the quasifission B_{qf} and intrinsic fusion B^*_{fus} barriers: at large angular momentum of dinuclear system B_{qf} decreases and B^*_{fus} increases. The large quasifission barrier increases the life-time of dinuclear system allowing it to transform into a CN [10]. It is concluded that the effects of competition between fusion and quasifission in the reaction play an important role in the dynamics process. The total evaporation residue and fusion-fission excitation functions are calculated in the framework of the advanced statistical model. The maximal value of the total cross section of the evaporation residue is 0.12 mb and fusion-fission cross section is comparable with the quasifission cross section. The contribution of the fast fission appears at $E_{c.m.} > 131$ MeV and it is sufficiently small in comparison with contributions of fusion-fission and quasifission reactions.

References

1. H. Q. Zhang *et al.*, Phys. Rev. C. **81**, 034611 (2010).
2. G. Keller *et al.*, Phys. Rev. C. **36**, 1364 (2010).
3. A. K. Nasinov *et al.*, Eur. Phys. J. A **34**, 325 (2007).
4. A. K. Nasinov *et al.*, Phys. Rev. C. **79**, 024606 (2009).
5. J. R. Huizenga *et al.*, Phys. Rev. **177** 1826 (1969)
6. G. Fazio *et al.*, Eur. Phys. Jour. A **19** 89 (2004).
7. G. Giardina *et al.*, Eur. Phys. J. A **8** 205 (2000).
8. S. Raman *et al.*, Atomic Data and Nuclear Data **36**, 1 (1987).
9. R. H. Spear *et al.*, Atomic Data and Nuclear Data **42** , No. 1, 55 (1989).
10. A. K. Nasirov, *et al.*, Nucl. Phys. A **759**, 342 (2005).
11. K. Pomorski *et al.*, Nucl. Phys. A **679** (2000) 253
12. A. D' Arrigo *et al*, Phys. Rev. C **46**, 1437 (1992).
13. A. D' Arrigo *et al*, J. Phys. G **20**, 365 (1994).
14. R. N. Sagaidak *et al*, J. Phys. G **24**, 611 (1998).